International Journal of Heat and Mass Transfer 52 (2009) 5802–5813

Contents lists available at ScienceDirect

International Journal of Heat and Mass Transfer

journal homepage: www.elsevier.com/locate/ijhmt

Enhanced boiling heat transfer in mesochannels

John D. Schwarzkopf [a], Steven G. Penoncello [b], Prashanta Dutta [a,*]

[a] School of Mechanical and Materials Engineering, Washington State University, Pullman, WA 99164-2920, USA
[b] Center for Applied Thermodynamic Studies, Department of Mechanical Engineering, University of Idaho, Moscow, ID 83844-0902, USA

ARTICLE INFO

Article history:
Received 9 June 2009
Received in revised form 17 July 2009
Accepted 17 July 2009
Available online 16 September 2009

Keywords:
Mesochannels
Minichannels
Enhanced boiling
Electronics cooling

ABSTRACT

Heat transfer characteristics are studied for a hybrid boiling case that combine features of spray cooling and flow boiling. In such a hybrid system, a liquid is atomized and the surrounding vapor is entrained into the droplet cone to provide an initial quality for enhanced boiling. An in-house experimental setup was developed to obtain surface temperature and heat flux measurements in a series of converged mesochannels for hybrid boiling. To compare the heat transfer performance of this hybrid technique, a flow boiling module was also developed using the same series of converged mesochannels. The inlet and exit hydraulic diameter of the mesochannels was 1.55 and 1.17 mm, respectively. The heat flux was in the range of 15–45 kW/m^2 and the estimated mass flux varied from 45 kg/m^{2}s at the channel inlet to 110 kg/m^{2}s at the channel outlet. Moreover, a model was presented to predict surface temperatures and heat transfer coefficients for flow boiling and hybrid boiling in mesochannels. This model was developed based on Chen's formulation (1966) [21] but with two essential modifications. First, the laminar entry length effect was taken into consideration for heat transfer coefficient calculation. Second, the boiling enhancement factor was calculated based on the fluid properties. The model was compared to the experimental data and several other correlations for both cases. This model shows good agreement with the experimental data (mean deviations on the order of 12–16%).

1. Introduction

In the field of electronics cooling, there is a demand for high heat flux cooling due to the increased waste heat and package density. Currently, air cooled heat sinks are widely used on electronic equipment due to reliability, safety, low cost and ease of maintenance. However, air cooled heat sinks are approaching a wall of limitation as electronic packaging becomes increasingly dense. This realization creates a need for advanced heat transfer methods.

Two-phase flows are being investigated and incorporated into the area of electronics cooling due to their superior heat transfer and increased heat removal limits. Chu et al. [1] reported that various two-phase mechanisms, such as pool boiling, convective flow boiling and spray cooling, have been tested for electronic cooling. Agostini et al. [2] showed that multi-phase technologies have the potential to remove higher density heat loads in electronics while maintaining the necessary junction temperature.

Among the various two-phase schemes, spray cooling has been shown to have higher heat transfer coefficients along with increased critical heat flux. In a spray cooling system, the heat acquisition process involves the combined effects of convection, boiling, and evaporation [3]. There have been several investigations of spray cooling with water and refrigerants [3–5] showing heat removal capabilities upwards of 1000 W/cm^2. Although spray cooling has much higher heat removal ability over pool boiling techniques [6], there are several drawbacks to spray cooling electronics such as increased complexity and difficultly managing the excess liquid within the spray region.

Flow boiling offers reduced complexity and improved fluid management around the heated region, but the heat transfer performance is much lower than spray cooling methods. Kew and Cornwell [7] studied various flow boiling heat transfer correlations for minichannels. They evaluated several correlations developed by Lui and Winterton [8], Cooper [9], Lazarek and Black [10], and Tran et al. [11] and compared them to experimental data; the deviations vary from 19% to 250%. Zhang et al. [12] developed a correlation for flow boiling heat transfer coefficients associated with low liquid Reynolds number in mesochannels. They compared the results with a wide range of experimental data; the mean deviation varied from 10.7% to 25.3%. Cheng and Mewes [13] reviewed the work on flow boiling with pure and mixture fluids in small channels. They concluded that although numerous studies have been published on boiling in small channels, few studies focused on the fundamentals of boiling at these smaller length scales.

Qu and Mudwar [14] studied flow boiling of water inside of microchannels. They evaluated 11 macroscopic correlations and compared them to their experimental data. For the correlations

* Corresponding author. Tel.: +1 509 335 7989; fax: +1 509 335 4662.
E-mail address: dutta@mail.wsu.edu (P. Dutta).

0017-9310/$ - see front matter © 2009 Elsevier Ltd. All rights reserved.
doi:10.1016/j.ijheatmasstransfer.2009.07.022

Nomenclature

c_{pl}	specific heat (liquid phase)
D	diameter
F	boiling augmentation factor
g	gravity
G	mass flux
h	heat transfer coefficient
h_{lv}	latent heat of vaporization
k	thermal conductivity of the fluid
L	length of channel
M	molecular mass
p	pressure
Pr	Prandtl number
R	universal gas constant
Re	Reynolds number
S_n	nucleation suppression factor
T	temperature
U	velocity
x	quality
X	Martinelli Factor
z	coordinate along channel length

Greek symbols

α	void fraction
α(T)	temperature function for Peng-Robinson equation of state
β	volume fraction of liquid
η	corresponding states factor
μ	dynamic viscosity
ν	kinematic viscosity
ρ	density
σ	surface tension
υ	specific volume
ω	acentric factor

Subscripts

c	critical
h	hydraulic
l	liquid phase
lam	laminar
mic	microscopic boiling
mac	macroscopic boiling
o	reference fluid (R-134a)
r	reduced
sat	saturation
tp	two-phase
tt	turbulent liquid and vapor
turb	turbulent
v	vapor phase
w	wall

evaluated, the mean absolute error varied from 19.3% to 272%. Their data show a decrease in the heat transfer coefficient with quality. Recently, Lee and Mudawar [15] studied subcooled boiling effects of a dielectric fluid (HFC 7100) in microchannels. They show that subcooling can increase the critical heat flux and claim that upwards of 700 W/cm^2 is capable without the risk of premature dryout. Ribatski et al. [16] evaluated over 2100 experimental data points for hydraulic diameters in the range of 200 μm to 3 mm (in the range of minichannels as described by Kandlikar [17]). They noted that large discrepancies were found in data gathered by independent researchers under similar conditions.

To circumvent the drawbacks of spray cooling yet utilize the advantages of flow boiling, a hybrid technique has been studied and reported by Schwarzkopf et al. [18]. This hybrid technique uses vapor entrainment to increase the convective boiling heat transfer coefficient in a series of mesochannels with varying aspect ratio throughout the length of the channel. To obtain the vapor entrainment, liquid is atomized and the high velocity droplets pump the surrounding vapor to create an initial quality at the onset of the mesochannels. The purpose of the initial quality is to promote annular flow throughout the length of the channel, resulting in increased heat transfer [19].

In a recent work [18], the momentum analysis for such a hybrid system is presented under the assumption that the momentum effects transition quickly to flow boiling and that the spray droplets entrain the surrounding vapor thereby pumping vapor into the channels and yielding an initial quality. The present work is focused on comparing and validating the concept of vapor entrainment as a mode of boiling enhancement. The rest of the paper is organized as follows. First, the experimental apparatus is described for both flow boiling and hybrid boiling. Then, the theory for modeling the heat transfer coefficients associated with flow boiling and hybrid boiling is developed. Next, the method for finding thermophysical properties of a dielectric fluid is presented. Finally, the experimental data for both flow boiling and hybrid boiling are presented and compared to the proposed model and other existing correlations.

2. Experimental setup

In order to understand the effects of vapor entrainment, a baseline must be established. In this study, flow boiling was selected as the baseline for comparison. Fig. 1 shows a schematic of the experimental apparatus used to characterize the flow boiling and vapor entrainment cases with a uniform heat flux. A dielectric fluid (PF5050) was used because of its chemical compatibility with materials used in the electronics industry and its low boiling point (30 °C at ~1 atm) to ensure minimal heat loss between the heat

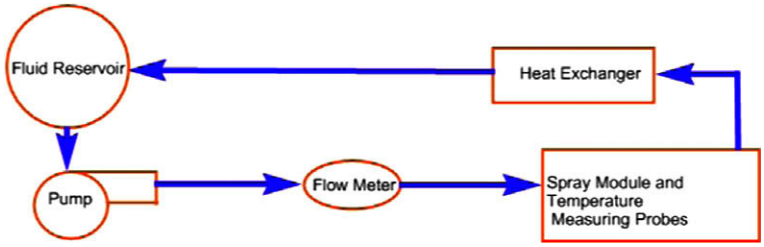

Fig. 1. Schematic of uniform heat flux experimental setup.

acquisition device and the ambient air. In the schematic, the two-phase fluid (PF5050) exits the spray module and travels up (~1 m) to an air-to-liquid heat exchanger to condense the fluid. The fluid is then routed to a reservoir where the non-condensable gases can be separated from the fluid and released to ambient through a pressure release valve. The single phase fluid is then routed down

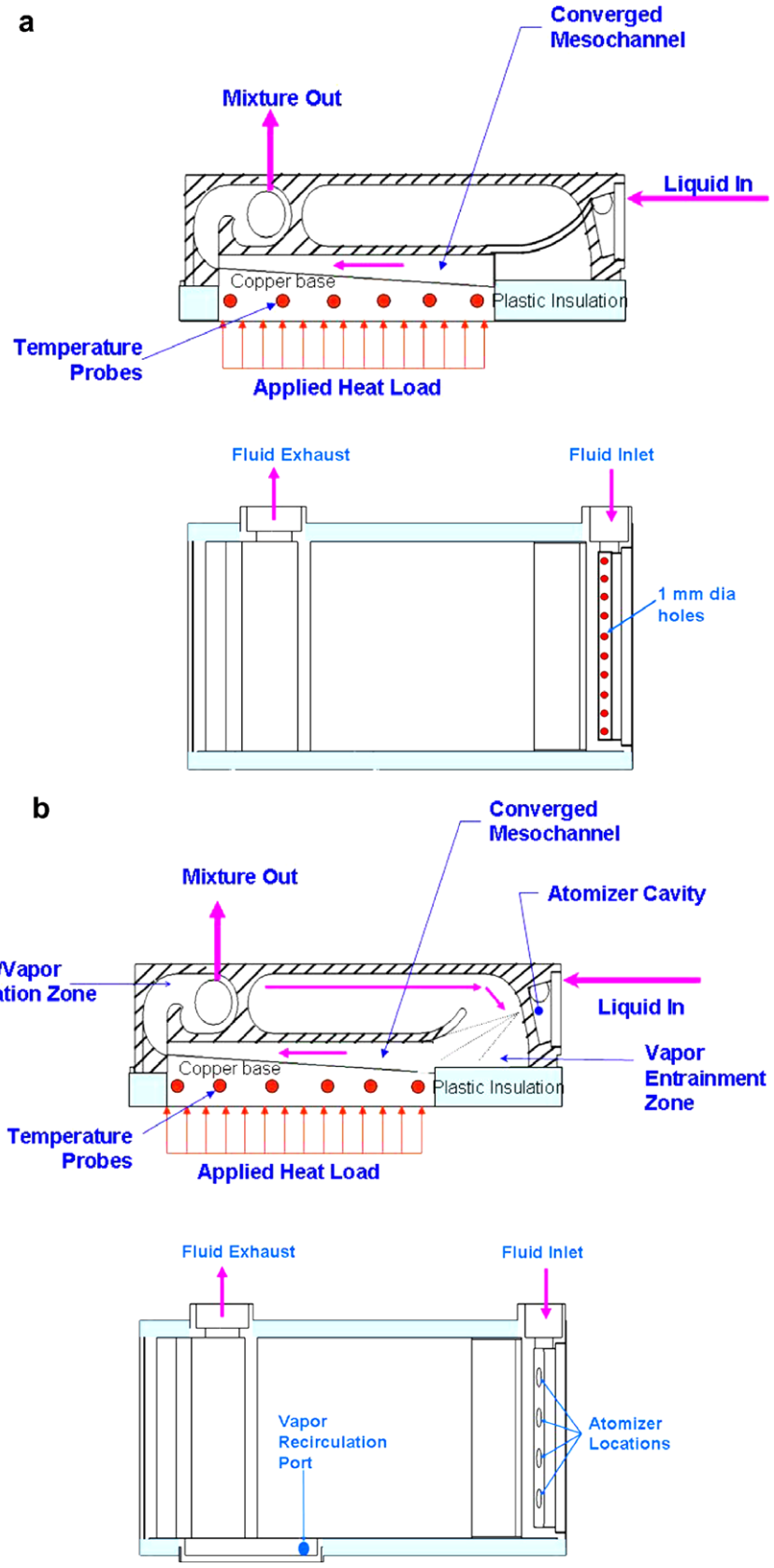

Fig. 2. Details of (a) flow boiling module and (b) vapor entrainment or hybrid module. In both cases, top figure shows side section view, while the bottom figure is the top section view.

Table 1
Fluid properties and flow characteristics.

	Flow boiling			Vapor entrainment		
	50 W	75 W	100 W	50 W	75 W	100 W
Liquid volumetric flow rate, mL/min	94	95	96	84	84	84
Saturation temperature, °C	33.3	33.6	34.4	32.1	32.3	32.8
Initial quality	0	0	0	9.8%	9.8%	9.8%

(~1 m) to the pump where it is pressurized and returned to the spray module. The purpose of the elevated heat exchanger was to prevent the pump from cavitating.

Fig. 2 shows the essential features of both the flow boiling and vapor entrainment modules. The flow boiling module contained a small inlet plenum with ten 1-mm diameter flat plate orifices that delivered fluid to an inlet plenum, shown in Fig. 2(a). The purpose of the ten 1 mm orifices was to reduce pressure surging within the module while providing evenly distributed flow to the channels. The pressure differential across the flow boiling module was approximately 0.05 bars.

The vapor entrainment module contained four full cone pressure swirl atomizers operating at 1.4 bar differential pressure, shown in Fig. 2(b). The full cone atomizers supplied high velocity liquid droplets in a vapor entrainment zone. These high speed droplets create a low pressure region causing the surrounding vapor to entrain into the spray. Vapor was supplied to the entrainment zone from a liquid/vapor separation zone in the exhaust region of the module. Due to the pressure difference, vapor was transported from the liquid/vapor separation zone through the vapor recirculation port and into the vapor entrainment zone (additional details and pictures of the vapor entrainment module are discussed elsewhere [20]).

Both modules contained 17 sloped channels milled into tellurium copper, each having inlet and exit hydraulic diameters of 1.55 mm and 1.17 mm, respectively. The finned geometry consisted of 18 fins each 500 μm thick and 33 mm long. The copper section with the channels was mounted in a polycarbonate housing to reduce lateral conduction away from the finned heat acquisition area, shown in Fig. 2(a and b). To provide a uniform heat flux at the base of the copper section, under the finned geometry, a thin film Kapton heater was mounted using a thermal interface material. A thick sheet of acetal was then used on the back side of the heater for insulation.

Six holes were drilled into the module base under the fins and 0.25 mm diameter type T sheathed thermocouples were installed. A thermocouple was positioned at the onset and exit of the channels and the remaining four thermocouples were equally spaced. The thermocouples reached to the center of the finned base plate where the highest temperatures were expected. Temperature and pressure measurements were made in the fluid stream at the inlet and exit of the spray module and the ambient temperature was measured at the inlet side of the fan (not shown) on the heat exchanger. The temperature, pressure and flow rate of dielectric fluid are shown in Table 1 for both vapor entrainment case and flow boiling case. The fluid flow rate was measured with a microturbine flow meter between the pump and the inlet of the module. The data acquisition device was a Keithley Model 2700. Data were taken until steady state was reached and then 50 samples or more were recorded and averaged.

The amount of heat loss to the environment was estimated using correlations for natural convection. The lid of the module was made out of aluminum and the walls are thin. Therefore it was assumed that the wall temperature was approximately equal to the fluid saturation temperature since the heat transfer coefficient for condensation inside of the module was much higher than the natural convection heat transfer coefficient on the outside of the module. Based on this assumption, the heat loss is estimated to be less than 1% of the heat load. The power to the heaters was calculated from voltage and current measurements, which was measured from a voltage drop across a known resistance. The voltage measurements were accurate to within ±0.01 mV. The uncertainty of the thermocouples was the greater of ±0.75% or ±1 °C.

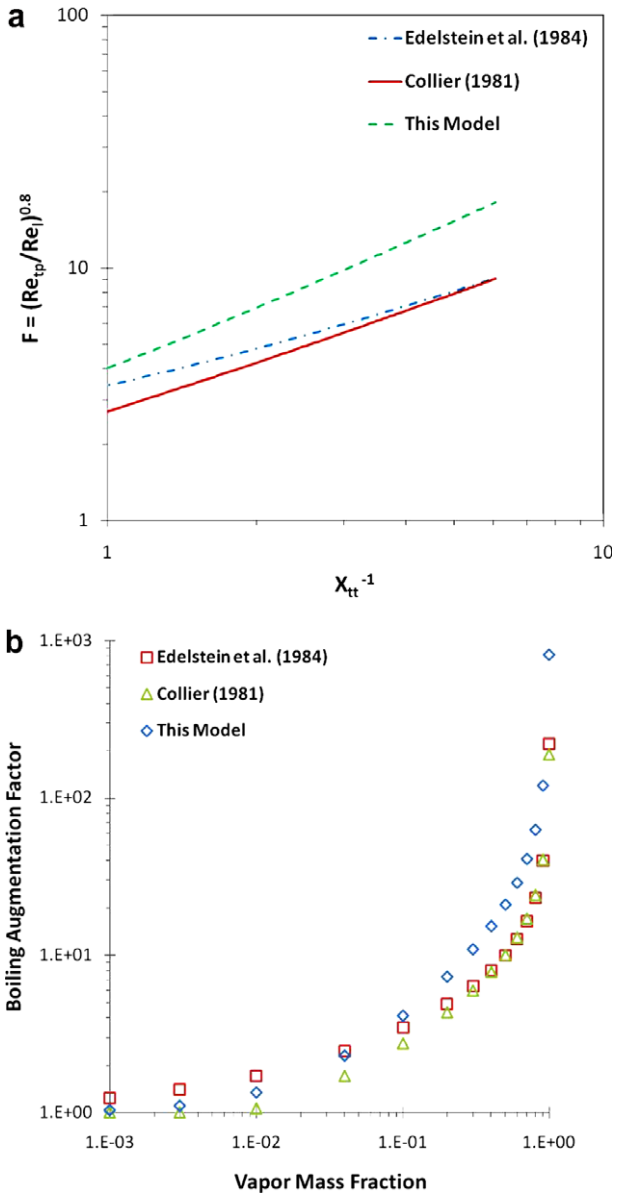

Fig. 3. Comparison of several boiling enhancement factors for a dielectric fluid (PF5050); (a) the proposed boiling enhancement factor, Eq. (17), is compared with the correlation by Collier [25], Eq. (8), and Edelstein et al. [27], Eq. (9), and (b) the three correlations show a singularity at a vapor mass fraction of unity.

The uncertainty of the absolute pressure gages were ±13.8 mbar. The maximum uncertainty in the flow rate was ±2 mL/min.

3. Theory

In order to understand the effect of vapor entrainment on heat transfer in mesochannels, a heat transfer correlation that is dependent on vapor mass fraction is necessary. Ideally, a correlation that would allow an initial quality at the inlet of the channels as a boundary condition is preferred. In the mid twentieth century, many correlations for flow boiling heat transfer coefficients were presented. Although the correlations seemed to accurately predict the data of the researcher, some of the correlations poorly predict the results from a different experiment. Chen [21] developed a correlation to predict the heat transfer coefficient independent of the data set. In the development, Chen [21] proposed a new method for modeling the physics of flow boiling. However, it included some empiricism to determine the nucleation suppression factor and the boiling augmentation factor which was correlated with data for vertical flow boiling in macrochannels. Moreover, Chen's model [21] was intended for macroscale boiling heat transfer where the Dittus-Boelter equation was used to obtain the convective heat transfer coefficient for fully developed turbulent flow. But within mesochannel boiling, the flow rate is much lower, therefore, a new model is proposed by considering laminar entry effects in mesoscale channels in addition to turbulent effects due to boiling. It is noteworthy to mention that this new model is not limited to vertical macroscale flow but rather extends the fundamentals of a previously proposed boiling model [21] to mesochannel flows.

3.1. Two-phase heat transfer coefficient

Chen [21] hypothesized that flow boiling heat transfer is a function of microconvection effects, which deals with bubble nucleation and growth, and macroconvection, which deals with bulk convective boiling. He then further assumes that these two modes of heat transfer are additive, where the two-phase heat transfer coefficient is of the form

$$h_{tp} = h_{mic} + h_{turb\_mac} \tag{1}$$

The microscopic heat transfer correlation is a modification to the Forster and Zuber [22] correlation for nucleate pool boiling. Chen [21] postulated that in the case of flow boiling, the bubble radius would decrease according to the liquid layer thickness. To account for the decrease in bubble radius, he proposed a suppression factor (S_n) to reduce the magnitude of the nucleate boiling term. The microconvection portion of the two-phase heat transfer coefficient was proposed as [21]

$$h_{mic} = 0.00122\left[\frac{k_l^{0.79}c_{pl}^{0.45}\rho_l^{0.49}}{\sigma^{0.5}\mu_l^{0.29}h_{lv}^{0.24}\rho_v^{0.24}}\right][T_w - T_{sat}(p_l)]^{0.24}[p_{sat}(T_w) - p_l]^{0.75}S_n \tag{2}$$

where the nucleation suppression term is modeled as [23,24]

$$S_n = \frac{[1-\exp\{-Fh_{turb}X_o/k_l\}]}{Fh_{turb}X_o/k_l} \tag{3}$$

and

$$X_o = 0.041\left[\frac{\sigma}{g(\rho_l-\rho_v)}\right]^{0.5} \tag{4}$$

To account for the increased heat transfer coefficient due to a thin layer of fluid on the wall, Chen [21] added a convective boiling term that increased in magnitude as the vapor mass fraction increased. Bennett and Chen [24] modified the macroscopic convective boiling term to account for Prandtl number effects; it is shown to be of the form

$$h_{turb\_mac} = h_{turb}F\left(\frac{\mathrm{Pr}_l+1}{2}\right)^{4/9} \tag{5}$$

where $\mathrm{Pr_l}$ is the liquid Prandtl number, F is the boiling augmentation factor defined as

$$F = \left(\frac{\mathrm{Re}_{tp}}{\mathrm{Re}_l}\right)^{4/5} \tag{6}$$

and h_{turb} is the liquid heat transfer coefficient for turbulent flows which can be obtained from the Dittus-Boelter equation

$$h_{turb} = 0.023\mathrm{Re}_l^{0.8}\mathrm{Pr}_l^{0.4}\left(\frac{k_l}{D_h}\right) \tag{7}$$

The boiling augmentation factor was originally determined from experimental data by Chen [21] and presented in graphical form as a function of the Martinelli factor. Based on the data of Chen [21], Collier [25] proposed the following correlation between the boiling augmentation factor and turbulent–turbulent Martinelli factor

$$\begin{aligned} F &= 1 && \text{for} \quad X_{tt}^{-1} \le 0.1 \\ F &= 2.35\left(0.213+\tfrac{1}{X_{tt}}\right)^{0.736} && \text{for} \quad X_{tt}^{-1} > 0.1 \end{aligned} \tag{8}$$

where X_{tt} is the turbulent–turbulent Martinelli factor [26]. Edelstein et al. [27] reported another form of the boiling augmentation factor

$$F = \left(1+\frac{1}{X_{tt}^{0.5}}\right)^{1.78} \tag{9}$$

One of the major drawbacks of Chen's formulation [21] is that the boiling augmentation factor was empirically found from flow boiling data of vertical macroscopic turbulent flows. It is preferred to have a model free from empiricism so that it can be used universally. In this study, a fundamental expression for the boiling enhancement factor is introduced and the work of Chen [21] is extended to include laminar and turbulent boiling effects typically found in mesoscale flows.

It is hypothesized that under certain circumstances, the laminar heat transfer coefficient for single phase flows may be larger than the fully developed turbulent heat transfer coefficient, especially in the entry length region, because of the low liquid Reynolds numbers associated with flows through a mesochannel. Moreover, it is assumed that the nucleate boiling and convective boiling terms can be summed, forming a two-phase heat transfer coefficient similar to Eq. (1). However, the microscopic and macroscopic effects are modified to account for entry effects and laminar effects of

Table 2
Fluid properties of PF5050 at a saturation temperature of 30 °C

Saturation pressure	Saturation temp.	Specific volume (m^3/kg)		Enthalpy kJ/kg		Viscosity (μPa s)		Thermal cond. (W/m K)		Surf. tens. (dyne/cm)	Prandtl number	
kPa	°C	Liq.	Vap.	Liq.	Vap.	Liq.	Vap.	Liq.	Vap.	Liq.	Liq.	Vap.
112.14	30	0.0005831	0.0735	56.54	144.30	527.3	11.97	0.051	0.012	9.06	10.09	0.753

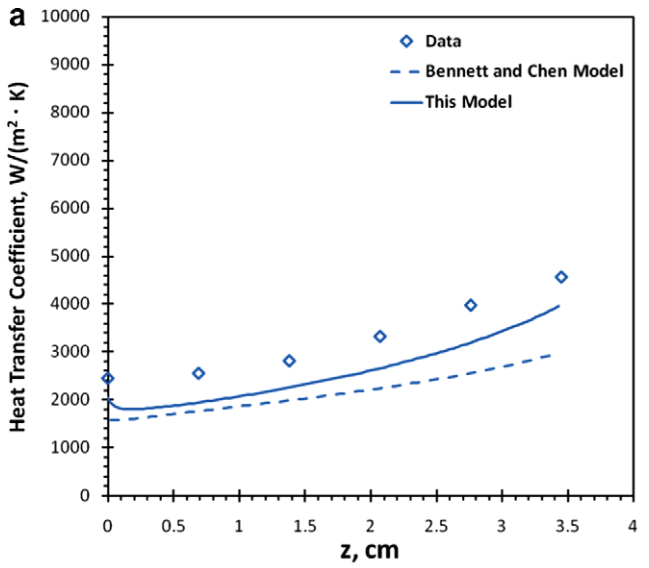

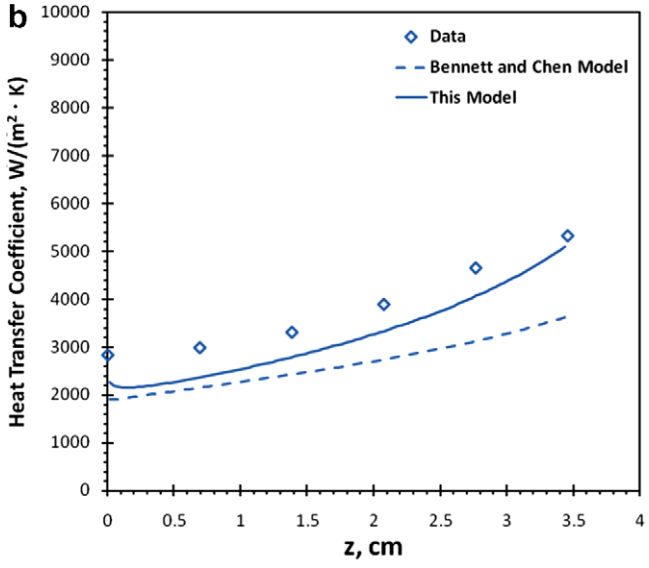

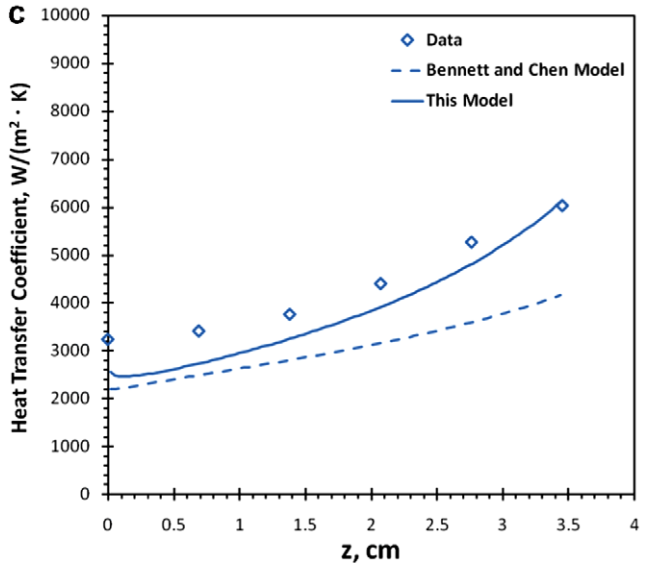

Fig. 4. Heat transfer coefficient distribution along the channel for flow boiling case. (a) 50 W, (b) 75 W, and (c) 100 W.

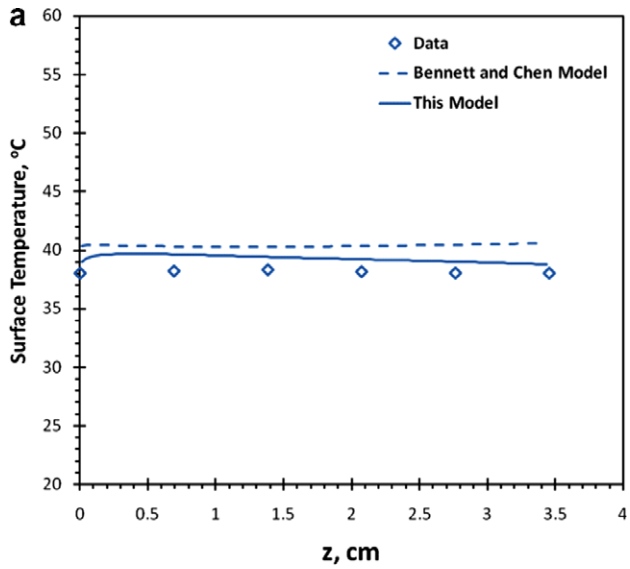

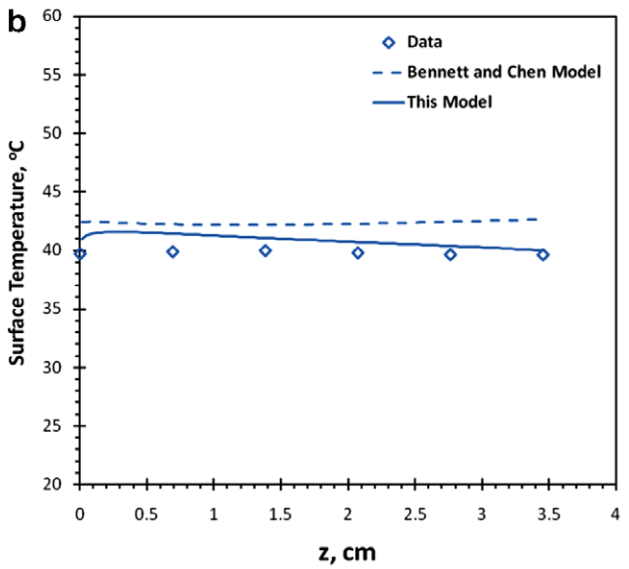

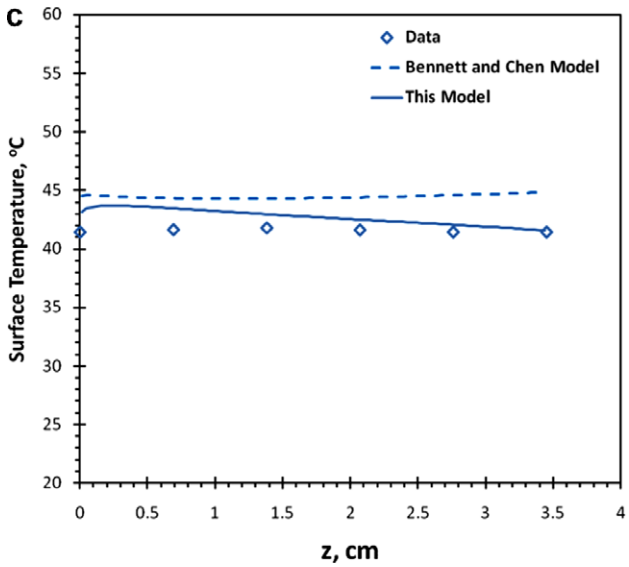

Fig. 5. Surface temperature distribution along the channel for flow boiling case. (a) 50 W, (b) 75 W, and (c) 100 W.

convective boiling. In order to accommodate for these effects, the overall two-phase boiling heat transfer coefficient is modified to be of the form

$$h_{tp} = h_{mic} + [(h_{turb\_mac})^2 + (h_{lam\_mac})^2]^{1/2} \tag{10}$$

where h_{mic} is described by Eq. (2) and the macroconvection term consists of turbulent and laminar contributions. The turbulent two-phase macroconvective heat transfer coefficient (h_{turb_mac}) is a modified version of the model proposed by Chen [21] and Bennett and Chen [24]. The laminar two-phase macroconvective heat transfer coefficient (h_{lam_mac}) is derived from the single phase local laminar entry length correlation proposed by Sieder and Tate [28]. The expression proposed by Sieder and Tate [28] is given as

$$h_{lam} = 1.24\frac{k_l}{D_h}\left(\frac{\mathrm{Re}_l\mathrm{Pr}_l}{z/D_h}\right)^{1/3}\left(\frac{\mu_l}{\mu_w}\right)^{0.14} \tag{11}$$

To formulate the two-phase heat transfer coefficient, the properties are converted to two-phase properties. The last term is neglected since the superheat in flow boiling is rather low. The two-phase laminar heat transfer coefficient can be expressed as

$$h_{lam\_mac} \approx h_{lam}\frac{k_{tp}}{k_l}\left(\frac{\mathrm{Re}_{tp}}{\mathrm{Re}_l}\frac{\mathrm{Pr}_{tp}}{\mathrm{Pr}_l}\right)^{1/3} \tag{12}$$

At this point, a similar argument to that of Chen [21] is proposed. As a first approximation, the liquid and two-phase thermal conductivity and Prandtl number are of the same order of magnitude and the ratio of the two-phase Reynolds number to the liquid Reynolds number is the dominant factor. With this assumption, the above equation is reduced to

$$h_{lam\_mac} = h_{lam}F^{5/12} \tag{13}$$

Substituting Eqs. (13) and (5) into (10) shows the two-phase heat transfer coefficient for flow boiling in mesochannels with an entry length effect of the form

$$h_{tp} = h_{mic} + \left[\left(h_{turb}F\left(\frac{1+\mathrm{Pr}_l}{2}\right)^{4/9}\right)^2 + (h_{lam}F^{5/12})^2\right]^{1/2} \tag{14}$$

Chen [21] described the two-phase Reynolds number in terms of liquid properties and a two-phase velocity

$$\mathrm{Re}_{tp} = \frac{\rho_l}{\mu_l}U_{tp}D_h \tag{15}$$

However, the above expression does not account for the effects of two-phase properties. The Chen correlation does not actually utilize the two-phase Reynolds number but rather uses the boiling augmentation factor as a function of the Martinelli parameter. This parameter is calibrated for macroscale flows but for mesoscale flows with a dielectric fluid, it may not be appropriate. To account for the effects of the two-phase Reynolds number, we have redefined the two-phase Reynolds number to be a function of two-phase properties as

$$\mathrm{Re}_{tp} = \left(\frac{\rho U}{\mu}\right)_{tp}D_h \tag{16}$$

The two-phase properties within the above expression can be easily determined. Using Eq. (16), an alternative expression for the boiling enhancement factor (F) is proposed as (details shown in Appendix A)

$$F = \left(\frac{\mu_l}{\mu_{tp}(1-x)}\right)^{4/5} \tag{17}$$

The above equation is plotted and compared to Eqs. (8) and (9) and shown in Fig. 3(a). The above equation shows to predict a much higher value of the boiling augmentation factor when compared to the empirical models proposed by Collier [25] and Edelstein et al. [27]. The proposed boiling augmentation factor (Eq. (17)) is also compared with Eqs. (8) and (9) as a function of the vapor mass fraction and shown in Fig. 3(b). Similar to the empirical models of Collier [25] and Edelstein et al. [27], the above equation also shows a singularity at a vapor mass fraction of unity. Although a singularity exists, it is safe to assume that critical heat flux will occur prior to a thermodynamic quality of unity. However, because of this singularity, a range of vapor mass fraction for this model is discussed later.

Substituting Eq. (17) into Eq. (14) reveals the final form of the two-phase model that accounts for low Reynolds number effects

$$h_{tp} = h_{mic} + \left[\left(h_{turb}\left(\frac{\mu_l}{\mu_{tp}(1-x)}\right)^{4/5}\left(\frac{1+\mathrm{Pr}_l}{2}\right)^{4/9}\right)^2 + \left(h_{lam}\left(\frac{\mu_l}{\mu_{tp}(1-x)}\right)^{1/3}\right)^2\right]^{1/2} \tag{18}$$

where h_{mic} is modeled by Eq. (2) and S_n is modified to be of the form

$$S_n = \frac{\left[1-\exp\left\{-\left(\frac{\mu_l}{\mu_{tp}(1-x)}\right)^{4/5}h_{turb}X_o/k_l\right\}\right]}{\left(\frac{\mu_l}{\mu_{tp}(1-x)}\right)^{4/5}h_{turb}X_o/k_l} \tag{19}$$

and X_o is modeled by Eq. (4). The single phase turbulent heat transfer coefficient (h_{turb}) is modeled by Eq. (7) and the single phase laminar heat transfer coefficient (h_{lam}) is modeled by Eq. (11). Within these equations, the single phase liquid properties are used and the liquid Reynolds number is defined as

$$\mathrm{Re}_l = \frac{G(1-x)D_h}{\mu_l} \tag{20}$$

where G is the mass flux. In order to understand the effect of the two-phase dynamic viscosity on convective flow boiling and hybrid boiling, a model is needed to predict this property for PF5050 at a given saturation temperature. Additional properties needed are the surface tension and thermal conductivity. The methods used to obtain these properties are described below.

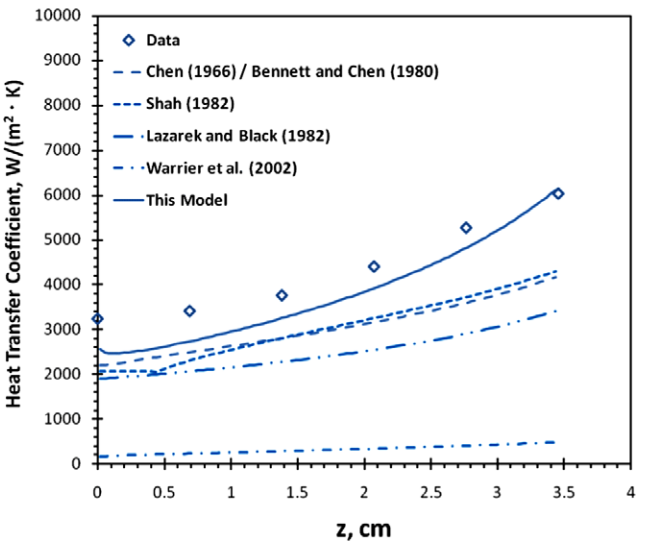

Fig. 6. Comparison of various correlations to the data for 100 W flow boiling case as a function of channel length.

4. The thermophysical properties

The thermodynamic properties for PF5050 are known at various pressures and temperatures, yet the transport properties are not well understood at pressures and temperatures above or below standard atmospheric conditions. In order to determine various parameters required in the formulation presented, the saturated liquid and saturated vapor dynamic viscosity and thermal conductivity as well as the surface tension are required.

The thermodynamic properties of the fluid were computed using a Peng-Robinson equation of state given by

$$p(\upsilon,T)=\frac{RT}{\upsilon-b}-\frac{a(T)}{\upsilon^2+2\upsilon b-b^2} \tag{21}$$

The parameters $a(T)$ and b are given by

$$a(T)=0.45724\alpha(T)\frac{R^2T_c^2}{p_c}\quad b=0.07779\frac{RT_c}{p_c} \tag{22}$$

The $\alpha(T)$ function for the Peng-Robinson equation of state is given by

$$\alpha(T)=[1+(0.37464+1.54226\omega-0.26992\omega^2)(1-T_r^{1/2})]^2 \tag{23}$$

In the above equations, critical properties are designated with a subscript 'c', properties reduced by the critical point value are indicated with a subscript 'r', and ω is the acentric factor for the fluid.

The dynamic viscosity, μ, is computed using a corresponding states approach developed by Huber et al. [29]. Using this model, the viscosity of a fluid is given by

$$\mu(\rho,T)=\mu^*(T)+\Delta\mu_o(\rho_o,T_o)\eta \tag{24}$$

The independent variables used to calculate the fluid viscosity are density and temperature. In a case where a different pair of independent, intensive properties is known, the Peng-Robinson equation of state for the fluid is used to compute the density and temperature that represent the thermodynamic state. The superscript '$*$' denotes the dilute gas viscosity which is determined from Chapman-Enskog theory. The residual viscosity is represented by $\Delta\mu_o(\rho_o,T_o)\eta$, where the subscript '$o$' refers to a reference fluid whose properties are accurately known. The factor η is given by

$$\eta=f^{1/2}n^{-2/3}\sqrt{\frac{M}{M_o}} \tag{25}$$

where f and n are equivalent substance reducing ratios determined from extended corresponding states theory, and M and M_o represent molecular masses. In the corresponding states calculations, the reference fluid viscosity is calculated using a formulation for Refrigerant 134a by Huber et al. [29].

The thermal conductivity formulation used was also developed by Huber et al. [29]. The thermal conductivity is given by

$$k(\rho,T)=k^{\mathrm{int}}(T)+k^{trans}(\rho,T) \tag{26}$$

As with the viscosity formulation, the independent properties are density and temperature. If other independent, intensive properties are known, a Peng-Robinson equation of state is used to find the density and temperature. The superscript 'int' refers to the internal molecular contribution and the superscript '*trans*' describes the thermal conductivity due to translational collisions between molecules. The translational thermal conductivity is made up of three parts

$$k^{trans}(\rho,T)=k^*(T)+k^{crit}(\rho,T)+k_o^r(\rho_o,T_o)\eta \tag{27}$$

In this equation, $k^*(T)$ is the dilute gas contribution, $k^{crit}(\rho,T)$ is the critical enhancement to the thermal conductivity and $k_o^r(\rho_o,T_o)\eta$ is the residual thermal conductivity. The internal molecular and dilute gas contributions to the thermal conductivity are calculated using standard classical expressions. The critical enhancement term is an adaptation of the critical crossover model developed by Olchowy and Sengers [30]. The subscript 'o' in the residual thermal conductivity represents the thermal conductivity of a well-known reference substance. In this work, the residual thermal conductivity is calculated using a formulation for Refrigerant 134a by Perkins et al. [31].

The surface tension is determined using a corresponding states method developed by Brock and Bird [32] and further modified by Miller [33]. The surface tension is given by

$$\sigma=p_c^{2/3}T_c^{1/3}J\left(1-\frac{T}{T_c}\right)^{11/9} \tag{28}$$

where

$$J=0.1196\left[1-\frac{(T_{NBP}/T_c)\ln(p_c/p_{atm})}{1-(T_{NBP}/T_c)}\right]-0.279 \tag{29}$$

In these expressions, the surface tension, σ, is given in [mN/m] or [dyne/cm], the temperatures are in [K], and pressures are in [bar]. The value of the normal boiling temperature, T_{NBP} is computed from the Peng-Robinson equation of state for the fluid at p_{atm} = 1.01325 bar.

5. Results and discussion

To provide a baseline for comparing the vapor entrainment data and evaluating several heat transfer correlations, a flow boiling experiment was used. The flow boiling module is described in the experimental setup; the flow rate, saturation temperature

Table 3
A comparison of correlations with the experimental data is shown for the 100 W flow boiling case (MD-FB) and the 100 W hybrid or vapor entrainment case (MD-VE), where MD is the mean deviation defined as $MD=\frac{1}{N}\sum_1^N\frac{|h_{exp}-h_{pred}|}{h_{exp}}\times 100\%$.

Reference	Correlation for two-phase heat transfer coefficient (h_{tp})	MD-FB (%)	MD-VE (%)
Chen [21] Bennett and Chen [24]	$h_{tp}=h_{mic}+h_{mac}$, h_{mic}, and h_{mac} are defined in Eqs. (2) and (5), respectively	29.4	37.7
Shah [35]	$h_{tp}=h_l{}^*\max(1.8\,\mathrm{N}^{-0.8},\varphi)$	30	39.3
	$\varphi=230\mathrm{Bo}^{0.5}$, $\mathrm{Bo}>0.3*10^{-4}$, $N>1.0$		
	$\varphi=1+46\mathrm{Bo}^{0.5}$, $\mathrm{Bo}\leqslant 0.3*10^{-4}$, $N>1.0$		
	$\varphi=\mathrm{F_s Bo}^{0.5}\exp(2.74\,N^{-0.1})$, $0.1<N\leqslant 1.0$		
	$\varphi=\mathrm{F_s Bo}^{0.5}\exp(2.47\,\mathrm{N}^{-0.15})$, $N\leqslant 0.1$		
	$F_s=14.7$, $\mathrm{Bo}\geqslant 11*10^{-4}$		
	$F_s=15.43$, $\mathrm{Bo}<0.3*10^{-4}$		
	$N=\mathrm{Co}$, $\mathrm{Fr}\geqslant 0.04$		
	$N=0.38\mathrm{Fr}^{-0.3}\mathrm{Co}$, $\mathrm{Fr}<0.04$		
Lazarek and Black [10]	$h_{tp}=30\,\mathrm{Re}^{0.857}\,\mathrm{Bo}^{0.714}\,\mathrm{k_l/D_h}$	42.2	53.7
Warrier et al. [34]	$h_{tp}=(1.0+6\mathrm{Bo}^{1/16}-5.3(1-855\mathrm{Bo})\times^{0.65})\,\mathrm{k_l/D_h}$	92.8	92.9
This model	$h_{tp}=h_{mic}+(h_{turb,mac}^2+h_{lam,mac}^2)^{1/2}$	12.9	16.5

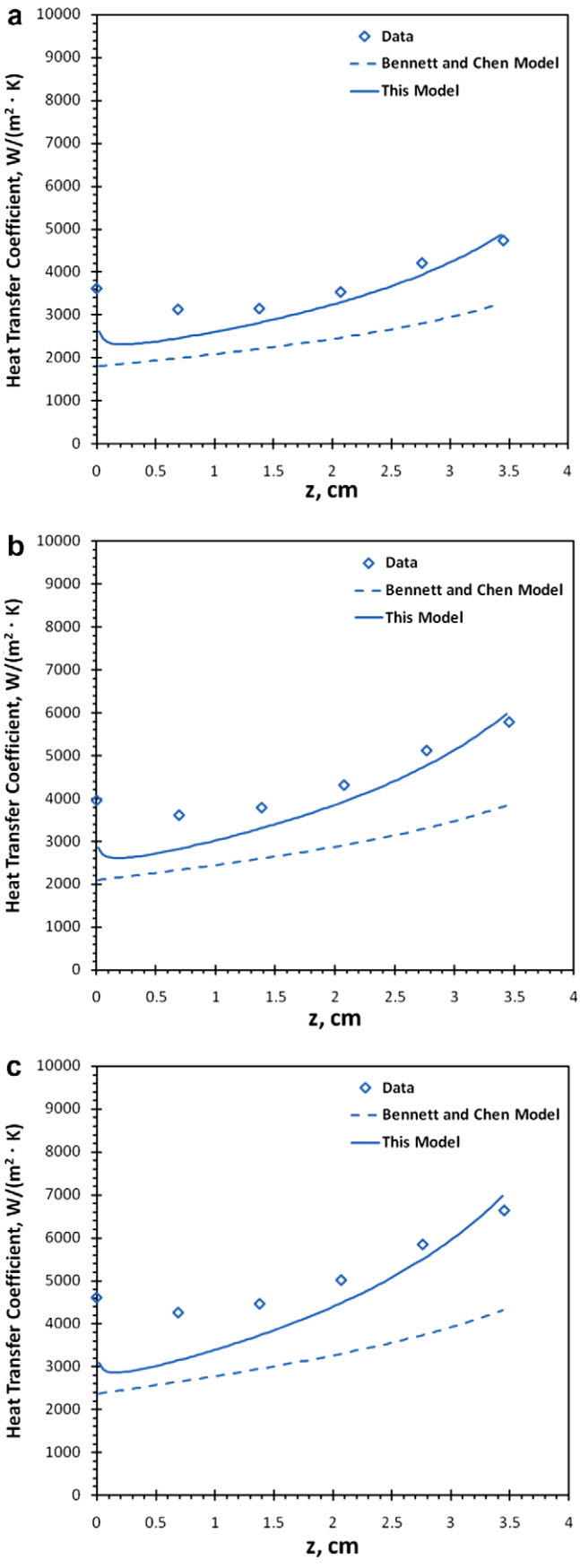

Fig. 7. Heat transfer coefficient distribution along the channel for hybrid boiling case. (a) 50 W, (b) 75 W, and (c) 100 W.

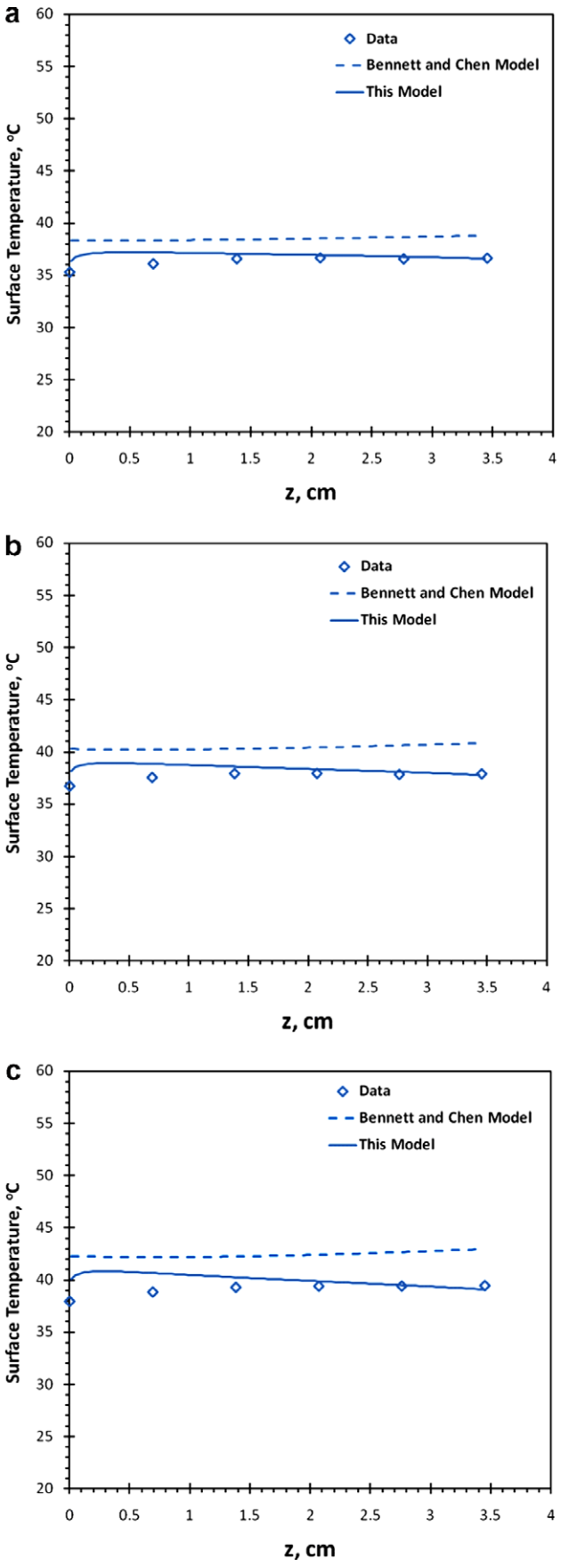

Fig. 8. Surface temperature distribution along the channel for hybrid boiling case. (a) 50 W, (b) 75 W, and (c) 100 W.

and initial quality are shown in Table 1. The heat transfer coefficients were found from the data by assuming that the heat was evenly distributed at the base of the module. The channel length was divided into six sections associated with the surface temperature measurements. The standard deviation of the six temperature measurements within the copper base was less than 0.25 °C, suggesting that lateral conduction can be neglected. The average fin efficiency was 94%, and thus it was assumed that the temperature was nearly constant throughout the fin. The heat flux was determined from the surface area and the assumption that the heat was evenly distributed. The surface superheat was determined from the difference between the measured surface temperature and the saturation temperature.

A quasi-one-dimensional model was used to model the heat transfer rate within the channels. This type of model assumes that the rate of change of the channel flow area is gradual such that flow separation does not occur. The change in surface and cross-sectional flow area is calculated at each step and an average hydraulic diameter was used between steps. The pressure drop inside the channels was deemed negligible [18]; thus a change in saturation temperature due to the pressure drop was not considered. Since the correlation for the microconvective boiling heat transfer coefficient (Eq. (2)) is a function of the surface temperature, the surface temperature was iterated until the residual was less than 0.001 °C. The fluid properties were calculated using the methods described in Section 4, and the results are shown in Table 2.

The flow boiling experiments were performed for 50, 75, and 100 W heat loads. The heat transfer coefficients are plotted and compared to the prediction of the current model (Fig. 4(a–c)). The original Bennett and Chen correlation [24] was also plotted for comparison. Although the Bennett and Chen model [24] gives reasonable results, this model captures the effects of increasing heat transfer coefficients with increasing quality and decreasing channel wall area in a non-equilibrium boiling environment [18]. The measured temperatures at the base of the channel are nearly uniform throughout the length of the channel, shown in Fig. 5(a–c). The predictions of the present model and the model of Bennett and Chen [24] are compared to the experimental data, and both models show a nearly uniform temperature.

The proposed model for boiling heat transfer coefficients in mesochannels is compared to other models that were developed for minichannels and macrochannels. Several popular correlations are those proposed by Lazarek and Black [10], Bennett and Chen [24], Warrier et al. [34], and Shah [35]. A comparison of the heat transfer coefficients along the channel length is shown in Fig. 6 for the 100 W flow boiling case. Surprisingly, the macroscopic correlations appear to reasonably predict the trends found from the experimental data in a mesochannel. The mean deviation for the 100 W flow boiling case ranges from 12.9% (the present model) to 92.8% (Warrier et al. [34]), both shown in Table 3, column three (MD-FB). The model of Tran et al. [11] and Yu et al. [36] were also evaluated but were not included because the deviations were significantly higher than those shown in Table 3. The correlations that appear to reasonably predict the experimental data are Bennett and Chen [24], Shah [35], and Lazarek and Black [10].

The hybrid cooling solution combines the benefits of spray cooling and flow boiling. This method of cooling relies on a superficial quality generated by an atomizer. The purpose of the atomization is to entrain the surrounding vapor and provide a mixture of vapor and liquid to the onset of the channel. This "initial quality" is hypothesized to give higher heat transfer coefficients throughout the channel when compared to flow boiling cases. The surface superheat and heat flux data was collected for the hybrid cooling module, which contained the same channel structure as the flow boiling module. The heat transfer coefficients were computed based on the measured heat, surface area, surface and saturation temperatures and are shown in Fig. 7(a–c) for heat loads of 50, 75, and 100 W. The hybrid cooling technique shows improved heat transfer along the length of the channel when compared to the flow boiling data. Since the lateral conduction is minimal and the heated surface area is decreasing, the momentum effects due to the vapor mass fraction must contribute to the increased heat transfer.

The measured heat transfer coefficients are plotted with the predictions of the present correlation and the Bennett and Chen correlation [24] and are shown in Fig. 7(a–c). When comparing these data to the flow boiling data (Fig. 4a–c), the increased heat transfer at the onset of the channel is due to the spray cooling effect. Toward the end of the channel, this model shows to accurately capture the effects of increasing heat transfer coefficients with increasing quality and decreasing channel wall area in a non-equilibrium boiling environment. The measured temperatures at the base of the channels are shown in Fig. 8(a–c) and are compared to the predictions of the present model and the model of Bennett and Chen [24].

The correlations for two-phase heat transfer coefficients provided by Lazarek and Black [10], Bennett and Chen [24], Warrier

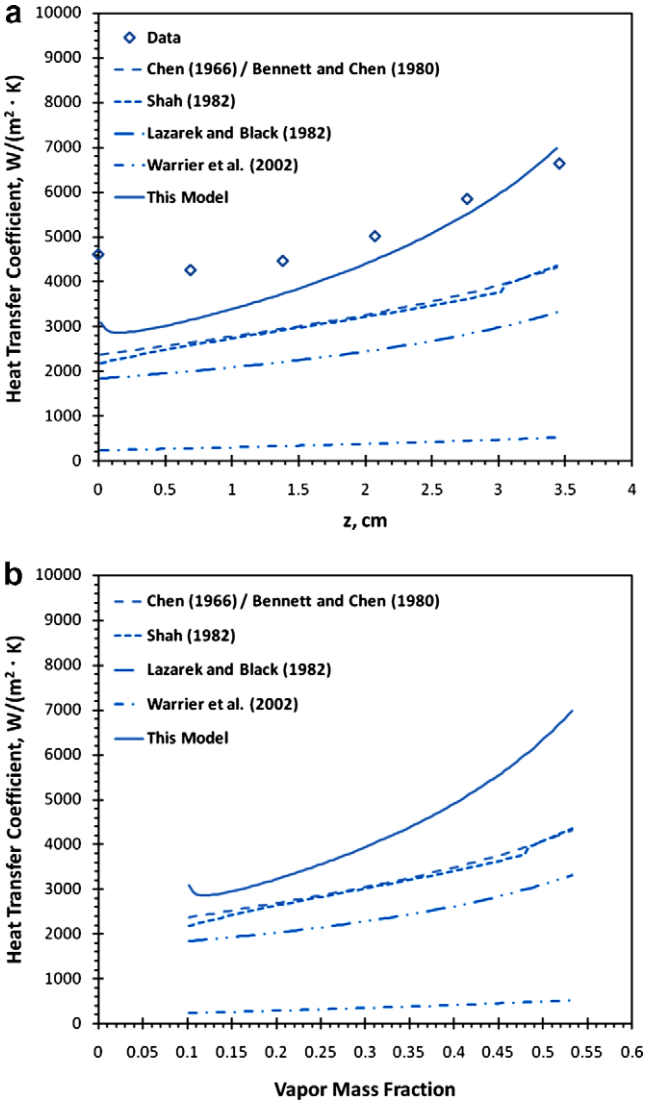

Fig. 9. Comparison of various correlations to the experimental data for 100 W hybrid boiling case (a) as a function of channel length and (b) as a function of vapor mass fraction.

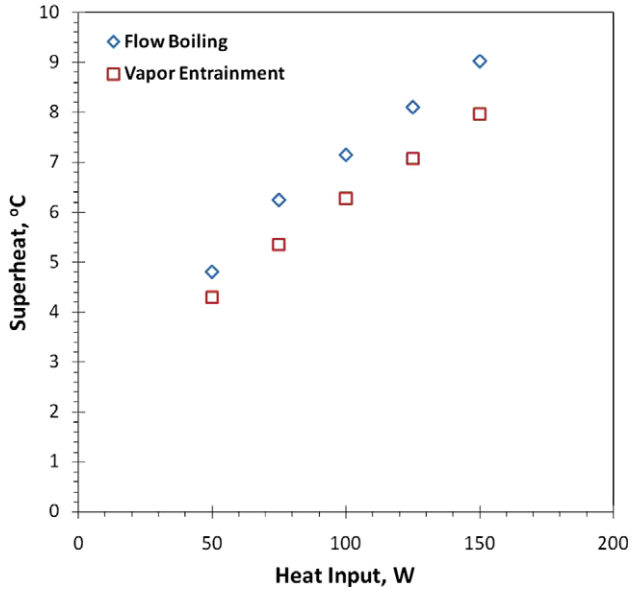

Fig. 10. Measured superheat comparison of flow boiling and hybrid boiling (vapor entrainment) for various uniform heat loads.

et al. [34], and Shah [35] are also compared with this model and the experimental heat transfer coefficients for the 100 W case (Fig. 9(a)). The experimental data show a unique trend. The heat transfer coefficient is moderate at the onset of the channel, decreases into the channel, and then transitions to an increase. The high heat transfer coefficient at the onset of the channel is partly due to entry length effects and partly due to spray cooling effects. In the entry region of the channel, the pressure gradient is positive, thus the atomized droplets are slowing down [18]. As the vapor velocity increases, the heat transfer coefficient increases, showing that quality is an important factor. In order to understand the effect of initial quality on these correlations, the heat transfer coefficients of five correlations are plotted against the quality within the mesochannel and are shown in Fig. 9(b). From this figure, it is clear that quality does affect the heat transfer, and it is noteworthy to mention that the boiling augmentation factor (F) provides adequate results up to a vapor mass fraction of 55%. The correlations of Bennett and Chen [24] and Shah [35] are close to matching the experimental data, but the present model shows to better capture the trends. The mean deviations are evaluated over the channel length and shown in Table 3 (column MD-VE) and vary from 16.5% (this model) to 92.9% (Warrier et al. [34]); again, the model of Tran et al. [11] and Yu et al. [36] were also evaluated but were not included because the deviations were significantly different than the above mentioned models.

The effects of vapor entrainment on the surface superheat for a heat range of 50–150 W are shown in Fig. 10. This figure clearly shows that providing an initial quality to the heated channels decreases the surface superheat which reflects an increase in the heat transfer coefficient for the same heat load. Overall, it has been shown that the current model under predicts the heat transfer coefficient at the onset of the channel but accurately predicts the heat transfer coefficient towards the end of the channel. The additional increase in heat transfer at the onset of the channel is likely caused by the atomized droplets impacting the finned area near the onset of the channels.

6. Concluding remarks

A new concept for a two-phase heat transfer is presented. This concept is based on a hybrid technique between spray cooling and flow boiling and focuses on pumping vapor into a series of mesochannels with a series of atomizers. The "initial quality" that is generated by this process shows enhanced heat transfer that can be applied to electronics cooling.

A new model for predicting two-phase heat transfer coefficients in minichannels or mesochannels is presented. This model includes the laminar effects that are typically found in minichannels or mesochannels, and it also includes a fundamental boiling enhancement factor that is not based on empiricism.

The model for the two-phase heat transfer coefficients is compared to both flow boiling experiments and vapor entrainment experiments. The model shows good agreement with experimental measurements and the overall comparison of heat transfer coefficients and surface temperatures are quite reasonable for two-phase flow. The model is also compared with two-phase heat transfer coefficient correlations developed by other researchers. The mean deviation is used to evaluate the performance of the models. This model is shown to better predict heat transfer coefficients for flow boiling cases with zero initial quality, and it also performs well in predicting the measured trends of flow boiling with an initial quality presented by atomization effects.

Acknowledgments

The authors are grateful to SprayCool, Inc. for providing funding to support this research. The authors credit Mr. Charles Tilton with the idea of the hybrid boiling/vapor entrainment technique (US patent 7,392,660) and thank Mr. Tilton and Dr. Don Tilton for their technical support.

Appendix A. Derivation of the boiling enhancement factor, *F*

The boiling enhancement factor is described as [21]

$$F = \left(\frac{\mathrm{Re}_{tp}}{\mathrm{Re}_l}\right)^{0.8} \tag{A1}$$

The two-phase Reynolds number can be defined as

$$\mathrm{Re}_{tp} = \left(\frac{U}{\nu}\right)_{tp} D \tag{A2}$$

The two-phase density can be written in terms of the specific volume as

$$\rho_{tp} = \frac{1}{x\upsilon_v + (1-x)\upsilon_l} = \frac{1}{\frac{x}{\rho_v} + \frac{(1-x)}{\rho_l}} \tag{A3}$$

Similarly, the two-phase dynamic viscosity can be written as [23]

$$\mu_{tp} = \frac{1}{\frac{x}{\mu_v} + \frac{(1-x)}{\mu_l}} \tag{A4}$$

The average liquid and vapor velocity can be expressed as

$$U_l = \frac{G(1-x)}{\rho_l \beta} \quad \text{and} \quad U_v = \frac{Gx}{\rho_v \alpha} \tag{A5}$$

where α and β are volume fractions of the vapor and liquid, respectively. From a mass balance, the two-phase velocity can be described as

$$U_{tp} = \frac{(\rho UA)_v + (\rho UA)_l}{(\rho A)_{tp}} = \frac{G}{\rho_{tp}} \tag{A6}$$

Substituting Eq. (A6) into (A2), the two-phase Reynolds number is described by

$$\mathrm{Re}_{tp} = \frac{GD}{\mu_{tp}} \tag{A7}$$

and the boiling enhancement factor (F) can be expressed as

$$F = \left(\frac{GD}{\mu_{tp}}\frac{\mu_l}{G(1-x)D}\right)^{0.8} = \left(\frac{\mu_l}{\mu_{tp}(1-x)}\right)^{0.8} \quad \text{(A8)}$$

References

[1] R.C. Chu, R.E. Simons, M.J. Ellsworth, R.R. Schmidt, V. Cozzolino, Review of cooling technologies for computer products, IEEE Trans. Device Mat. Reliab. 4 (4) (2004) 568–585.

[2] B. Agostini, M. Fabbri, J.E. Park, L. Wojtan, J.R. Thome, B. Michel, State of the art of high heat flux cooling technologies, Heat Transfer Eng. 28 (2007) 258–281.

[3] D.P. Rini, R.H. Chen, L.C. Chow, Bubble behavior and nucleate boiling heat transfer in saturated FC-72 spray cooling, J. Heat Transfer 124 (2002) 63–72.

[4] D.E. Tilton, Spray Cooling, Ph.D. Dissertation. University of Kentucky, Lexington, KY, 1989.

[5] I. Mudawar, K.A. Estes, Optimizing and predicting CHF in spray cooling of a square surface, J. Heat Transfer 118 (1996) 672–679.

[6] D.P. Rini, R.H. Chen, L.C. Chow, Bubble behavior and heat transfer mechanism in FC-72 pool boiling, Exp. Heat Transfer 14 (2001) 27–44.

[7] P.A. Kew, K. Cornwell, Correlations for the prediction of boiling heat transfer in small-diameter channels, Appl. Therm. Eng. 17 (1997) 705–715.

[8] Z. Lui, R.H.S. Winterton, A general correlation for saturated and subcooled flow boiling in tubes and annuli based on a nucleate boiling equation, Int. J. Heat Mass Transfer 34 (1991) 2759–2766.

[9] M.G. Cooper, Saturated nucleate pool boiling – a simple correlation, IChemE Symp. Ser. 86 (1984) 785–793.

[10] G.M. Lazarek, S.H. Black, Evaporative heat transfer, pressure drop and critical heat flux in a small vertical tube with R113, Int. J. Heat Mass Trans. 25 (1982) 945–960.

[11] T.N. Tran, M.W. Wambsganss, D.M. France, Small circular- and rectangular channel boiling with two refrigerants, Int. J. Multiphase Flow 22 (1996) 485–498.

[12] W. Zhang, T. Hibiki, K. Mishima, Correlation for flow boiling heat transfer at low liquid Reynolds number in small diameter channels, J. Heat Transfer 127 (2005) 1214–1221.

[13] L. Cheng, D. Mewes, Review of two-phase flow and flow boiling of mixtures in small and mini channels, Int. J. Multiphase Flow 32 (2006) 183–207.

[14] W. Qu, I. Mudawar, Flow boiling heat transfer in two-phase micro-channel heat sinks – I. Experimental investigation and assessment of correlation methods, Int. J. Heat Mass Transfer 46 (2003) 2755–2771.

[15] J. Lee, I. Mudawar, Fluid flow and heat transfer characteristics of low temperature two-phase micro-channel heat sinks – Part 1: experimental methods and flow visualization results, Int. J. Heat Mass Transfer 51 (2008) 4315–4326.

[16] G. Ribatski, L. Wojtan, J.R. Thome, An analysis of experimental data and prediction methods for two-phase frictional pressure drop and flow boiling heat transfer in micro-scale channels, Exp. Thermal Fluid Sci. 31 (2006) 1–19.

[17] S.G. Kandlikar, Fundamental issues related to flow boiling in minichannels and microchannels, Exp. Thermal Fluid Sci. 26 (2002) 389–407.

[18] J.D. Schwarzkopf, C.T. Crowe, P. Dutta, B.Q. Li, Atomized non-equilibrium two-phase flow in mesochannels: momentum analysis, Int. J. Heat Fluid Flow 30 (2009) 99–107.

[19] J.D. Schwarzkopf, C.L. Tilton, C.T. Crowe, B.Q. Li, A low profile thermal management device for high power processors using enhanced flow boiling techniques and perfluorocarbon fluids, in: ASME Summer Heat Transfer Proceedings, HT 2005-72527, San Francisco, CA, 2005.

[20] J.D. Schwarzkopf, M.S. Thesis, Washington State University, Pullman, WA, 2005.

[21] J.C. Chen, Correlation for boiling heat transfer to saturated fluids in convective flow, Ind. Eng. Chem. Process Des. Dev. 5 (1966) 322–329.

[22] H.K. Forster, N. Zuber, Dynamics of vapor bubbles and boiling heat transfer, AIChE J. 1 (1955) 531–535.

[23] V.P. Carey, Liquid–Vapor Phase-Change Phenomena, Hemisphere, New York, 1992.

[24] D.L. Bennett, J.C. Chen, Forced convective boiling in vertical tubes for saturated pure components and binary mixtures, AIChE J. 26 (3) (1980) 454–461.

[25] J.G. Collier, Forced convective boiling, in: A.E. Bergles, J.G. Collier, J.M. Delhaye, G.F. Hewitt, F. Mayinger (Eds.), Two phase flow and heat transfer in the power and process industries, Hemisphere, New York, 1981.

[26] R.W. Lockhart, R.C. Martinelli, Proposed correlation of data for isothermal two-phase, two-component flow in pipes, Chem. Eng. Prog. 45 (1949) 39–48.

[27] S. Edelstein, A.J. Perez, J.C. Chen, Analytic representation of convective boiling functions, AIChE J. 30 (1984) 840–841.

[28] E.N. Sieder, G.E. Tate, Heat transfer and pressure drop of liquids in tubes, Ind. Eng. Chem. 28 (1936) 1429–1435.

[29] M.L. Huber, A. Laesecke, R.A. Perkins, Model for the viscosity and thermal conductivity of refrigerants, including a new correlation for the viscosity of R134a, Ind. Eng. Chem. Res. 42 (2003) 3163–3178.

[30] G.A. Olchowy, J.V. Sengers, A simplified representation for the thermal conductivity of fluids in the critical region, Int. J. Thermophys. 10 (1989) 417.

[31] R.A. Perkins, A. Laesecke, J. Howley, M.L.V. Ramires, A.N. Gurova, L. Cusco, Experimental thermal conductivity values for the IUPAC round-Robin sample of 1,1,1,2-tetrafluoroethane (R134a), NISTIR 6605, National Institute of Science and Technology, Dec. 2000.

[32] J.R. Brock, R.B. Bird, Surface tension and the principle of corresponding states, AIChE J. 1 (1955) 174.

[33] D.G. Miller, On the reduced Frost-Kalkwarf vapor pressure equation, Ind. Eng. Chem. Fundam. 2 (1963) 78.

[34] G.R. Warrier, V.K. Dhir, L.A. Momoda, Heat transfer and pressure drop in narrow rectangular channel, Exp. Therm. Fluid Sci. 26 (2002) 53–64.

[35] M.M. Shah, Chart correlation for saturated boiling heat transfer: equations and further study, ASHRAE Trans. 88 (1982) 185–196.

[36] W. Yu, D.M. France, M.W. Wambsganss, J.R. Hull, Two-phase pressure drop, boiling heat transfer, and critical heat flux to water in a small-diameter horizontal tube, Int. J. Multiphase Flow 28 (2002) 927–941.